Forehead or Headlights – At Which Height Should LiDARs be Mounted on the Vehicle?

Kezhi Li, Yeqiang Qian, *Member, IEEE*, Chunxiang Wang, and Ming Yang, *Member, IEEE*

***Abstract*—An increasing number of production vehicles are opting to integrate LiDAR systems to achieve superior perception capabilities. However, there are significant differences in the installation positions, particularly the heights, of LiDAR systems across different car models from various companies. For instance, some are installed on the forehead of the vehicle, while others are mounted near the headlights. The installation height of LiDAR has a significant impact on its perception capability, including the LiDAR detection ability and the performance of 3D object detection algorithms. To investigate the influence of LiDAR installation height, we introduced the Height3 dataset, which is collected simultaneously by LiDAR sensors with three heights in the CARLA simulation environment. Using this dataset, we first conducted a comprehensive statistical analysis of the LiDAR detection ability and compared the number of detected vehicles and the detection rate of LiDARs at three heights. Furthermore, we investigated the impact of point clouds captured from different heights on the performance of multiple 3D vehicle detection algorithms. Based on the studies on the simulated Height3 dataset, we have an overall understanding of the performance differences of commercial vehicle-mounted LiDARs installed at different heights, providing suggestions for the installation positions of LiDAR sensors on production vehicles. The dataset is available on http://www.kaggle.com/datasets/kezhili/height3.**

***Index Terms*—Autonomous automobiles, 3D object detection, LiDAR height, simulated dataset.**

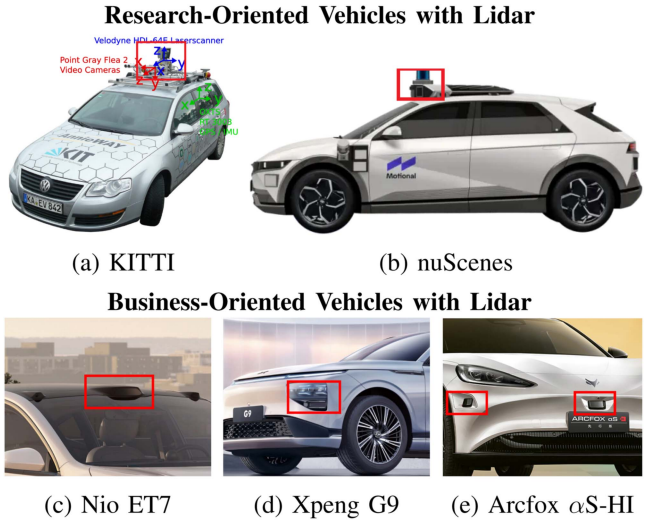

Fig. 1. (a) and (b) illustrate the LiDARs' mounting positions of vehicles in KITTI and nuScenes. (c) illustrates the LiDAR sensor of Nio ET7, which is embedded on the forehead of the car and roughly 1.6 m above the ground. (d) illustrates the LiDAR sensor of Xpeng G9, which is integrated into the car's headlights and roughly 0.6 m above the ground. (e) illustrates the LiDAR sensor of Arcfox αS-HI, which is installed directly above the license plate and roughly 0.4 m above the ground.

I. Introduction

LIDAR, as one of the most popular emergent detectors equipped on the newly released intelligent vehicle models, has stimulated the advanced improvement of the autonomous driving technologies [1]. The first appearance of LiDAR in the field of autonomous driving took place during the DARPA Grand Challenge [2], where a vehicle equipped with LiDAR technology showcased by Velodyne achieved impressive results [3]. This event paved the way for a remarkably promising future for LiDAR in the intelligent vehicle industry, leading to a surge in the development of state-of-the-art LiDAR technology [4], [5]. Thanks to the advent of solid-state hybrid LiDAR sensors [6], [7], [8], which replaced costly mechanical rotor-based LiDAR sensors [9] (Fig. 1(a) and (b)), the mass production and integration of LiDAR into commercial vehicles had been realized. Presently, industrial automotive-grade LiDAR systems have become market favorites for automobile companies. According to the official information released at the 2023 Shanghai Automobile Industry Exhibition, it has been announced that 38 new car models were equipped with LiDAR technology.[1]

As LiDAR is so vital in offering superior depth perception and distance measurement of the vehicle's surrounding environment [10], there is a crucial yet often overlooked variable that has a significant impact on the performance of LiDAR, which is the initial installation height of the LiDAR sensor. By

Manuscript received 11 July 2023; revised 21 August 2023 and 10 September 2023; accepted 18 September 2023. Date of publication 25 September 2023; date of current version 23 February 2024. This work was supported in part by the National Natural Science Foundation of China under Grant 62103261/62173228/U22A20100, and in part by the 2022 Open Project Program of Guangxi Key Laboratory of Automobile Components and Vehicle Technology under Grant 2022GKLACVTKF03. *(Corresponding authors: Yeqiang Qian; Ming Yang.)*

Kezhi Li is with the University of Michigan-Shanghai Jiao Tong University Joint Institute, Shanghai Jiao Tong University, Shanghai 200240, China (e-mail: little_black@sjtu.edu.cn).

Yeqiang Qian is with the Innovation Center of Intelligent Connected Electric Vehicle, Global Institute of Future Technology, Shanghai Jiao Tong University, Shanghai 200240, China (e-mail: qianyeqiang@sjtu.edu.cn).

Chunxiang Wang and Ming Yang are with the Department of Automation, Shanghai Jiao Tong University, Shanghai 200240, China, and also with the Key Laboratory of System Control and Information Processing, Ministry of Education, Shanghai 200240, China (e-mail: wangcx@sjtu.edu.cn; mingyang@sjtu.edu.cn).

Color versions of one or more figures in this article are available at https://doi.org/10.1109/TIV.2023.3318628.

Digital Object Identifier 10.1109/TIV.2023.3318628

[1]https://www.autoshanghai.org/?lang=en

TABLE I
LARGE VARIATIONS ON THE LIDAR INSTALLATION HEIGHT OF VEHICLE MODELS FROM DIFFERENT BRANDS

Place	Model[2]	FOV(°)	Distance(m)	Resolution(°)	Height(m)
Forehead	Leading Ideal L8	120×25	200	0.1×0.2	1.8
	AITO M5	120×25	150	0.25×0.26	1.6
Headlight	Xpeng G9	120×25	150	0.2×0.2	0.6
	NETA S	120×25	150	0.25×0.26	0.5
License Plate	Arcfox αS-HI	120×25	150	0.2×0.2	0.4
	AVATR 3	120×25	150	0.25×0.26	0.4

examining the installation configurations of LiDAR sensors on multiple commercially available vehicle models in recent years, it becomes apparent that there are noticeable variations in their mounting heights (see Table I). Almost all LiDAR sensors used by automotive companies have the same field of view (FOV), with subtle differences in sensing distance and resolution. However, different from the research-oriented LiDAR sensors that were usually mounted on the roof of the vehicles (Fig. 1(a) and (b)), the mounting height of the business-oriented LiDARs changes from 1.8 m to 0.4 m above the ground, encompassing multiple positions such as the vehicle's forehead, headlights and license plate (Fig. 1(c), (d), and (e)).

As there is such a big difference in the installation heights of multiple LiDAR sensors, we'd like to investigate the impacts of the height of LiDAR sensors in two aspects: (1) How does the detection ability of LiDAR sensor itself vary with the variation of its mounting height? The detection ability of LiDAR here represents the number of ground truth objects the LiDAR can detect. (2) LiDAR sensors at different heights capture the point cloud from varying angles, leading to variations in the shape of the captured point clouds from the same object. Besides, the number of points from objects scanned by LiDARs with different heights may be different. The differences in point cloud shapes and the number of points in the objects probably impact the learning of object features by algorithm models, leading to variations in the predicted results of the models. These possible influences of LiDAR height emphasize the importance of investigating the performance difference of LiDARs with different heights.

Some researchers used optimization algorithms to find the optimal LiDAR installation configurations on a vehicle [11], [12], [13], [14]. As none of them specifies their study on the impacts of installation height, the range of variation in their LiDAR sensor heights is not as significant as that of LiDAR heights in current commercial vehicles. For example, some of them only considered the LiDARs on the vehicle's roof, while some mounted their LiDARs in specific positions with little freedom to move. Besides, all of them specified their studies only on the research-oriented LiDARs, such as the rotor-based Velodyne LiDARs. The rotational LiDARs often have a 360° horizontal FOV. This makes the optimal mounting position always prone to be the top of the vehicle in order to fully use the potential of such an FOV. However, the commercial solid-state LiDARs are quite different from them for their limited FOVs and fixed positions. Moreover, none researched LiDAR height's influence on the perception tasks. Regarding the author's knowledge, this article is the first to focus on the influence of business-oriented LiDAR's mounting height on the LiDAR detection ability and perception tasks.

To investigate the influence of varying installation heights of LiDAR sensors, we collected a dataset named Height3 in the CARLA simulation environment using LiDAR sensors set at three different heights. The Height3 dataset is necessary for our analysis because it includes the point clouds collected simultaneously by LiDAR sensors with different heights. Besides, unlike traditional real-world scene datasets, the dataset collected in the simulation environment allows us to capture ground truth information for all vehicles in the environment, not only the vehicles detected by LiDAR. Through all the vehicles in the environment, we can analyze how many of these vehicles are detected by the LiDAR sensor and directly compare the LiDAR detection rate of different heights. Although the synthetic data have some drawbacks and cannot replace realistic data in real-world applications [15], [16], we use them here for comparison purposes and the specific need of our experiment.[3]

Based on the Height3 dataset, we studied the perception ability of LiDAR sensors in two aspects. Firstly, we analyzed the LiDAR detection ability of the total environment vehicles, i.e., the proportion of environmental vehicles from which the LiDAR can capture points. In the second stage, we analyzed the performance of perception tasks on the vehicles detected by LiDAR. Among all the perception tasks, we chose the classical 3D object detection task and assessed the performance of different 3D vehicle detection algorithms based on multiple feature extraction methods on our dataset.

The contributions of this research can be summarized as follows:

- We collected the Height3 dataset encompassing point clouds acquired from LiDARs with varying heights, which can provide a valuable resource for research in LiDAR installation height.
- We presented a comprehensive research report on the perception abilities of LiDARs with different installation heights, including the LiDAR detection ability and the performance of different 3D object detection algorithms on the vehicles detected by LiDAR.
- Starting from the actual environment of the vehicles, we analyzed all vehicles in the surroundings, compared to the traditional analysis only based on the vehicles already detected by LiDAR. Then, we particularly focused on the ones posing the greatest threat to the ego vehicle.

II. RELATED WORKS

A. 3D Object Detection

Perception tasks based on 3D point clouds, like object detection [17], [18], [19], [20], [21], [22], [23], [24], [25], [26], [27], [28], [29], [30], [31] and semantic segmentation [32], [33], [34], have achieved considerable advancements thanks to the power of deep neural networks. This article, specifically, will focus on the impact of LiDAR heights on 3D vehicle detection, which is a special case of 3D object detection.

As the methods shown in [24], [25], [26], [27] have proved to be efficient in indoor 3D object detection task, the objective of the outdoor 3D object detection is to detect and accurately locate various objects in the vicinity of a vehicle, including

[2]https://www.autoshanghai.org/?lang=en

[3]The dataset is available on http://www.kaggle.com/datasets/kezhili/height3

vehicles, bicycles and pedestrians [35]. Over the years, it has witnessed remarkable achievements. The pillar-based approach tackles this task by incorporating point cloud features within an infinitely high rectangular pillar [19], [20]. This projection technique transforms the 3D point cloud into a 2D plane from a top-down perspective. The features extracted from the 2D plane are subsequently processed using methods akin to those employed in 2D image analysis. Likewise, the voxel-based method divides the point cloud scene into discrete, finite-height voxels, effectively constructing a "3D" image [17], [18], [28], [29]. To overcome the information loss associated with the aforementioned methods, PointNet [36] directly extracts features from individual points. This innovation gained popularity in the advancement of point-based end-to-end algorithms [21], [22] as well as algorithms that utilize a mixture of data representations [30], [31].

Recently, the transformer model architecture, commonly used in Natural Language Processing (NLP), has demonstrated remarkable effectiveness in the field of computer vision as well [37]. Sheng et al. [23] introduced CT3D, an abbreviation for Channel-wise Transformer based two-stage 3D object detection framework, specifically designed for outdoor scenes. CT3D operates as a two-stage detector, employing the Region Proposal Network (RPN) from [18] to generate initial proposal boxes. Subsequently, channel-wise transformer encoder and decoder architectures are utilized to aggregate point features and facilitate contextual interactions. Finally, the Feed-Forward Networks leverage the transformer architecture's large receptive field to provide a more accurate prediction result.

B. Outdoor 3D Point Cloud Dataset

Most of the aforementioned end-to-end outdoor designed 3D object detection algorithms are primarily trained and evaluated using real-scene outdoor datasets [38], [39], [40], [41], [42], [43]. These datasets offer a wealth of data encompassing diverse real-world road and weather conditions, object classes, and numerous detected objects.

However, in our research, the limitation of these datasets is that they were not collected by LiDAR sensors installed at different heights. In KITTI [38], NuScenes [39], Once [41], H3D [42], and Argoverse [43], LiDAR sensors were mounted at the top of the ego vehicle to collect point clouds.

The Waymo dataset [40] partially addresses this limitation by utilizing five LiDAR sensors positioned in locations that encompass popular installation positions in current production cars. However, it does not provide separate point clouds for different installation heights and positions. As a result, it remains difficult to thoroughly analyze the effects of LiDAR installation heights on 3D object detection.

C. Researches on LiDAR Installation Configurations

Many researchers have conducted studies on the optimal installation configuration of LiDAR sensors on vehicles. The installation configuration here primarily includes the position coordinates of the LiDAR, as well as the rotation angle on three orientations and other parameters. Most of them employ optimization algorithms to find the best parameters for the LiDAR installation configuration.

By rasterization of the region of interest, Liu et al. [11] and Mou et al. [12] define the optimization task as minimizing the undetected areas within the area of interest. On the other hand, Berens et al. [13] and Kim et al. [14] choose to maximize the LiDAR occupancy grid by using a genetic algorithm to find the optimal solution. Their research provides algorithmic support for finding the optimized installation configuration of LiDAR and is a valuable reference for research on the installation height of LiDAR sensors on production vehicles.

However, these studies have some limitations on the research of LiDAR installation height. [11], [14], and [13] only considered a limited range of the height of LiDAR sensors. [11]'s LiDAR height only varied from 2.2 m to 3 m. [14] had four LiDAR sensors that were fixed in four specific positions with only a little freedom to move. [13] mounted their LiDARs on the roof of the vehicle. Although [12] gave their optimal results for the LiDAR's installation position, the position was not aligned with the positions of nowadays LiDAR sensors on commercially available cars. Besides, their results were very sensitive to the choice of the interested regions and the definition of the perception capability of LiDAR. Thus, if the region or the definition changes, the optimal results will change. Therefore, it is necessary to conduct experiments on abundant traffic scenarios and focus on the statistical results.

TABLE II
SETUPS FOR LIDAR SENSORS USED FOR DATASET COLLECTION. THE "CHANNEL" COLUMN REPRESENTS "VERTICAL CHANNEL" × "HORIZONTAL CHANNEL"

Height(m)	Distance(m)	VFOV(°)	HFOV(°)	Channel	Frequency (Hz)
1.8	150	-15∼10	180	128×480	20
1.0	150	-12.5∼12.5	180	128×480	20
0.5	150	-12.5∼12.5	180	128×480	20

III. THE HEIGHT3 DATASET

A. Basic Setup

We utilized the CARLA simulation environment to generate point clouds captured by LiDARs installed at different heights. The reason for using the CARLA simulation environment is not only because it can provide abundant LiDAR data from different heights simultaneously at a relatively lower time and cost, but also because it can offer information that cannot be obtained from real-world scenarios. For example, different from the datasets collected in realistic scenes that only record the ground truth objects detected by the LiDAR, our dataset recorded the total vehicles in the environment, allowing for the analysis of what proportion of vehicles in the surround of the ego vehicle that the LiDAR can detect.

Specifically, we collected data frames simultaneously using LiDARs at three distinct heights. The highest installation position we observed in current mass-produced cars was 1.8 m, while the lowest height was set at 0.5 m. Additionally, for comparative purposes, we added an extra LiDAR at 1.0 m, positioned approximately in the middle of the car's front windshield. The detailed configurations for the three LiDAR setups are presented in Table II.

To align with mainstream configurations, we adjusted the 1.8 m LiDAR downward by 2.5°, with a total vertical FOV of 25°. The other two LiDARs were positioned horizontally, also with a vertical FOV of 25°. We observed that mass-produced cars

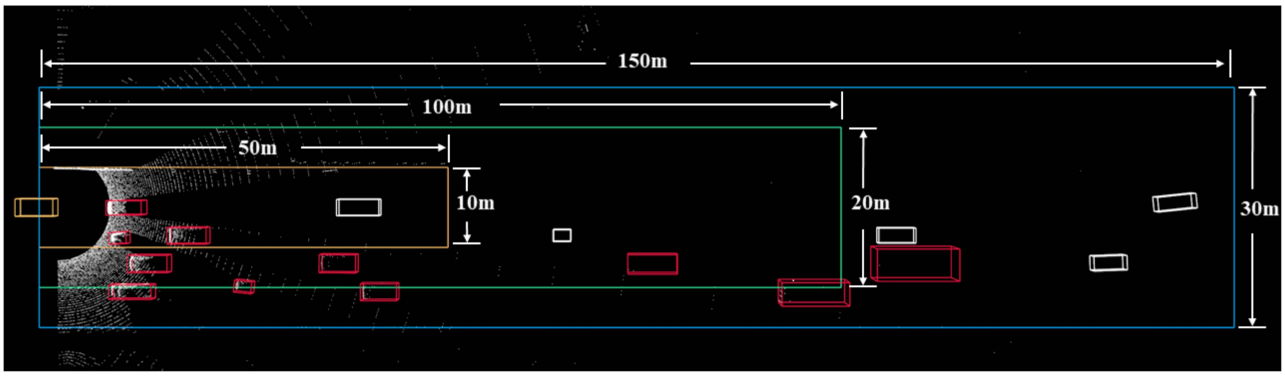

Fig. 2. This point cloud figure is from the height "1.8 m". The blue box represents the "Large range", which is $150m \times 30\,m$. The green box represents the "Moderate range", which is $100m \times 20\,m$. The yellow box represents the "Small range", which is $50m \times 10\,m$. The vehicles with red boxes are detected vehicles, while the white boxes correspond to undetected vehicles.

typically have two main installation schematics. One is that two LiDARs were installed with an FOV of 120°, which combines to form a 180° FOV. The other is that one LiDAR with 120° FOV is mounted at the forehead of the car. To have a trade-off between the two LiDAR setups, and specifically focus on the difference of LiDAR heights, the horizontal FOV of our LiDAR was set to 180° for LiDARs at all three heights. Moreover, since the CARLA simulation environment only has the rotational LiDAR sensor, we only simulated the solid-state LiDAR sensor through the FOV deduction. However, to achieve a more realistic simulation and provide more reliable experimental results, we are still pursuing a simulation method to mimic the scan pattern of solid-state hybrid LiDAR sensors like [44], other than the rotational version.

Our dataset was collected using the official map "Town04_Opt", which provides a simulated setting for a highway scenario. The dataset comprises a total of 8000 data frames, divided into 40 distinct scenes. Each scene is initialized with different environmental setups and consists of 200 data frames. During collection, 1 data frame was saved when 10 data frames were collected by LiDARs. Therefore, the data saving frequency is 2 frame/s since the original frequency is 20 frame/s. To streamline the analysis process and ensure efficiency, we chose to only place vehicle objects in our scene, including various types of vehicles such as cars, trucks, and taxis. We randomly placed 250 to 300 vehicles in the whole map across each scene so that the number of vehicles surrounding the ego vehicle is at a rational range. All the vehicles' behaviors were controlled by the "autopilot" mode of CARLA.

B. Range

Since we recorded all the environmental vehicle objects during the dataset-collecting process, we'd like to split them based on different metrics to support our analysis.

Considering the difference in the detection abilities of LiDARs with different heights may vary due to the definition of the detection range, we categorized the surrounding vehicles into three ranges with the ego car serving as the origin of the coordinate system.

The "small range" covers a range where $0 \leq x \leq 50$ and $-5 \leq y \leq 5$, with the y-axis covering the length of one lane on either side. The "moderate range" encompasses a wider area, where $0 \leq x \leq 100$ and $-10 \leq y \leq 10$, with the y-axis covering the length of two lanes on either side. Finally, the "large range" extends even further, covering $0 \leq x \leq 150$ and $-15 \leq y \leq 15$, corresponding to the length of three lanes on either side, and x reaches the maximal range of our LiDAR. The details are shown in Fig. 2.

C. Importance Level

In a real traffic scenario, not all vehicles around the ego vehicle are equally important. Different heights of LiDAR sensors may have significant variations in perceiving vehicles of different importance levels. Therefore, we introduced two metrics, namely "Top3" and "Top6," to classify the cars in traffic based on their level of importance (see Fig. 4).

We defined the "Top3" and "Top6" mainly on the vehicles' distance to the ego vehicle because these close vehicles are of great importance in lane-change or cut-in scenes. The "Top3" vehicles are considered the most important vehicles that the ego vehicle must detect, and also the vehicles that pose the greatest threat to the ego vehicle. They consist of one nearest vehicle in the left lane of the ego vehicle's lane, one nearest vehicle in the right lane, and the nearest vehicle in the ego line. If the left lane or right lane does not exist, we do not count the vehicle in that lane. Therefore, the Top3 vehicles do not always have 3 vehicles. On the other hand, the "Top6" vehicles represent the secondary level of importance and consist of the two closest vehicles in each of the left lane, right lane, and ego lane. Consequently, the "Top3" vehicles are a subset of the "Top6" vehicles.

IV. LiDAR Detection Ability

In the first stage of our experiment, we aimed to gain insights into the detection ability of LiDAR sensors with different heights. More specifically, we counted the number of objects, particularly cars, that the LiDARs could detect from the environment. We defined that if the LiDAR captured at least one point from a vehicle, the vehicle can be considered as "detected" by the LiDAR. Otherwise, it should be considered "undetected". Specifically, to prevent ground points from being mistakenly counted as points in the vehicle, we reduced the height of the vehicle's bounding box from the ground by 0.05 m. Then, we

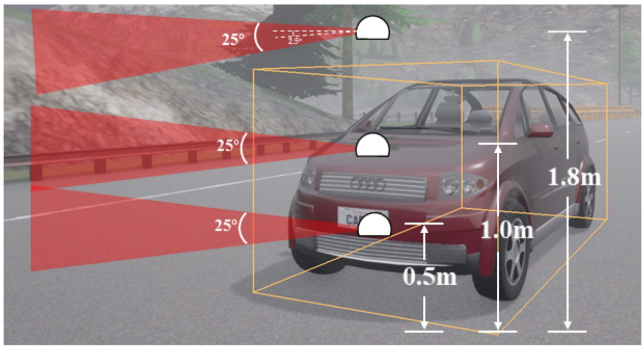

(a) LiDAR sensor setup for our data collection platform.

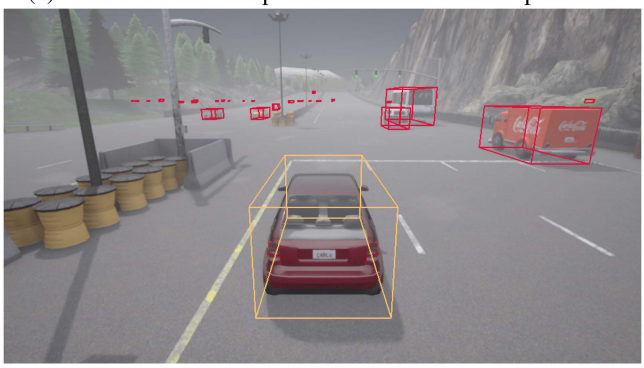

(b) LiDAR point clouds collected in the highway scenario.

Fig. 3. Visualization of the making process of the Height3 dataset.

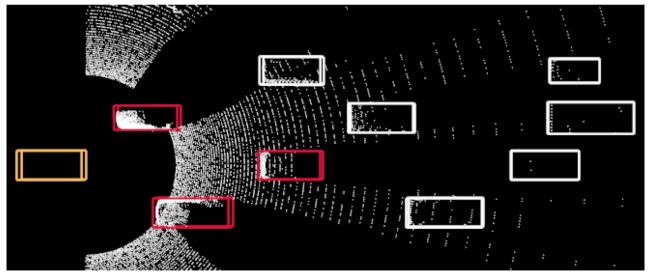

(a) Top3 Vehicles

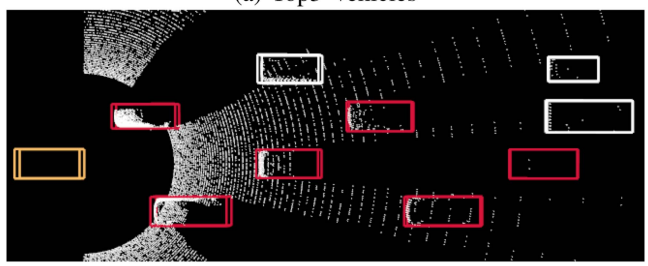

(b) Top6 Vehicles

Fig. 4. Visualization of Importance Level "Top3" and "Top6" on point cloud. The yellow box represents the ego vehicle. The red boxes are the corresponding "Top3" or "Top6" vehicles. The white boxes represent the other vehicles.

analyzed and compared the results using the metrics of "range" and "importance level" as described before. All detailed results are shown in Tables IV, V and VI.

A. Qualitative Analysis on LiDAR Detection Ability

For qualitative analysis, Fig. 5 visually presents the detected and undetected vehicle boxes by LiDAR sensors with different heights. It is evident that the red boxes, representing the detected vehicles, are much more prevalent in the 1.8 m point clouds compared to the 1.0 m and 0.5 m heights. As the height decreases from 1.8 m to 1.0 m or 0.5 m, some vehicles become undetected due to occlusion. This observation suggests the unparalleled advantage of the forehead-mounted LiDAR in avoiding occlusions. On the other hand, other lower heights likely exhibit similar perception capabilities since they suffer from the same occlusion situation, even if they have a 0.5 m height difference.

B. Vehicles Detected by LiDARs in Different Heights and Ranges

Fig. 6 shows the statistical results for the number of all detected environmental vehicles by the LiDAR sensors and the corresponding LiDAR detection rates under different ranges.

In Fig. 6(a), when considering the number of detected vehicles by LiDAR sensors, the 1.8 m height setting demonstrates a competitive ability to detect a significantly higher number of vehicles compared to the other two heights. This advantage becomes more pronounced as the detection range expands. Conversely, there is only a marginal difference in the number of detected vehicles between the 0.5 m and 1.0 m heights, even as the detection range increases.

We define the LiDAR detection rate (LDR) as:

$$LDR = \frac{Detected\ Num}{Total\ Num}. \tag{1}$$

In Fig. 6(b), the LDRs of all heights drop due to the range expanding. This result aligns with our expectation that it becomes more difficult for the LiDAR sensor to detect vehicles at a further range due to the limitation of LiDAR detection range and object occlusion. However, all three rates have decreased by the same magnitude. Although the LiDAR with a height of 1.8 m still exhibits a significant advantage compared to the other two heights, this advantage does not increase as the range expands. This is because as the range increases, the total number of vehicles also increases. This result reflects the relatively stable LiDAR detection rate differences among the three LiDARs under the range variation.

C. Vehicles Detected by LiDARs in Different Heights and Importance Levels

Fig. 7 shows the statistical results for the number of detected vehicles by the LiDAR sensors and the corresponding LiDAR detection rates with different heights under different importance levels.

Fig. 7(a) shows that at the "Top3" importance level, the differences in the number of detected vehicles by LiDARs with different heights are very small. This result suggests when only considering the "Top3" vehicles in the environment, the LiDAR detection abilities of different heights are close. The disparity becomes larger as the importance level becomes lower.

In Fig. 7(b), the LDRs of all heights decrease as the importance level decreases. The results align with the expectation that general vehicles are harder to detect than the important vehicles

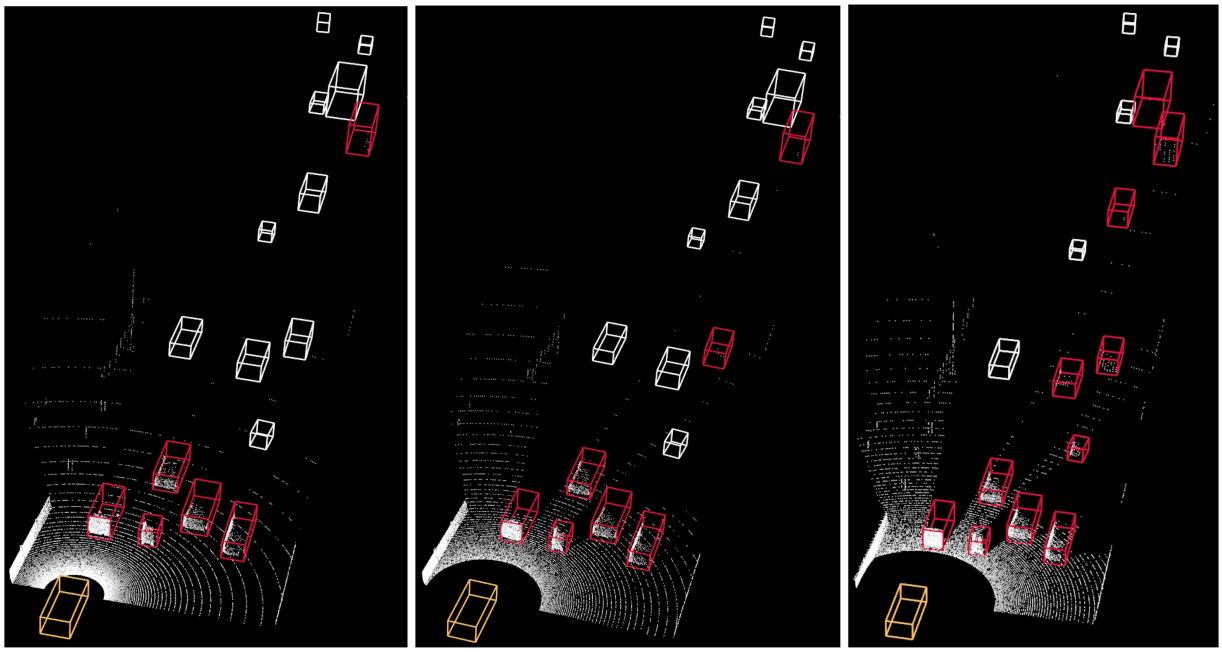

(a) 0.5m (b) 1.0m (c) 1.8m

Fig. 5. Point clouds visualization with different LiDAR heights. The left picture represents the LiDAR with 0.5 m. The middle one is collected by 1.0 m LiDAR. The right figure corresponds to the LiDAR of height 1.8 m. The white color vehicles represent the vehicles that are not scanned by the LiDAR lasers, which means there are no points in these boxes. The red boxes corresponding to the detected vehicles contain at least one point. The yellow box represents the ego vehicle.

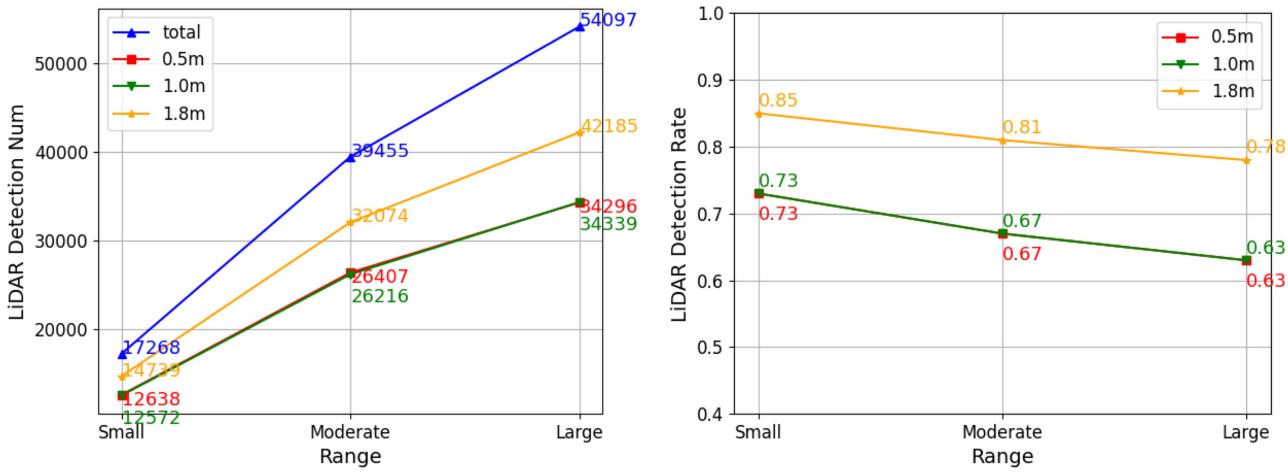

(a) The number of detected vehicles (b) The LiDAR detection rate

Fig. 6. Number of detected vehicles by LiDAR sensors and the corresponding detection rate with different heights in different ranges.

close to the ego vehicle. The more important the vehicles, the easier they are to be detected. Besides, the LDRs of the two lower heights decrease more than that of the height of 1.8 m. This disparity suggests that less important vehicles are more susceptible to occlusion, rendering them more challenging for the lower-height LiDAR to detect. As the importance level increases, the disparity between the 1.8 m and the other two heights becomes smaller. In "Top6" vehicles, there is still a noticeable superiority of height 1.8 m on the number and the detection rate. When considering the "Top3" vehicles, all three LiDAR heights demonstrate excellent and comparable results.

V. Performance of 3D Object Detection Algorithms

In the second stage of our experiment, we trained and tested multiple 3D object detection algorithms using ground truth vehicles that were successfully detected by LiDARs. The influence of the points' detection height on the performance of the 3D object detection algorithm may vary due to different data representation paradigms or backbone architectures. For example, the pillar-based method aggregates features through a pillar with infinite height, possibly making it less sensitive to the change of LiDAR detection height. Conversely, the voxel-based algorithm

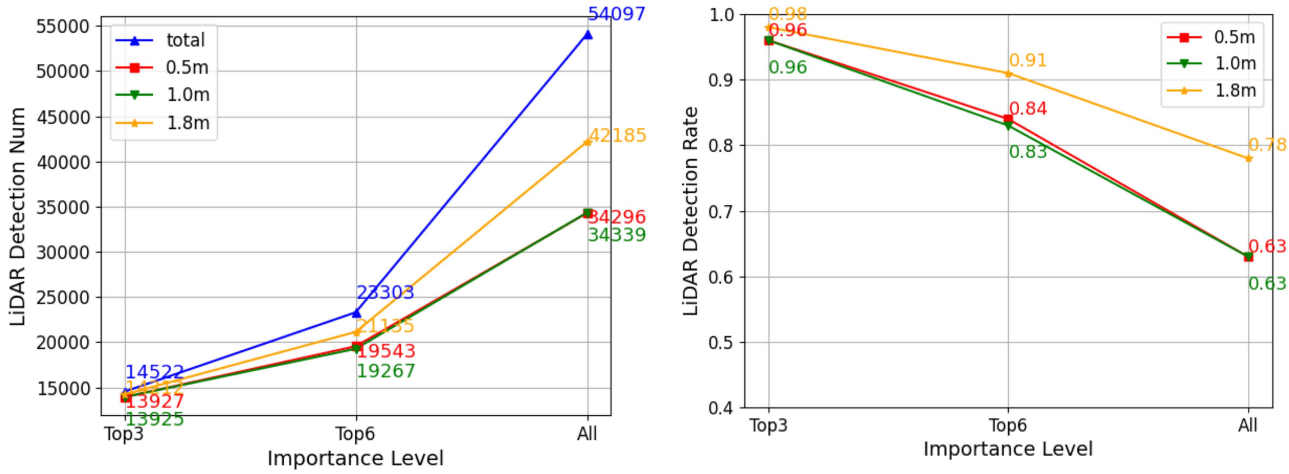

(a) The number of detected vehicles (b) The LiDAR detection rate

Fig. 7. Number of detected vehicles by LiDAR sensors and the corresponding detection rate with different heights in different importance levels.

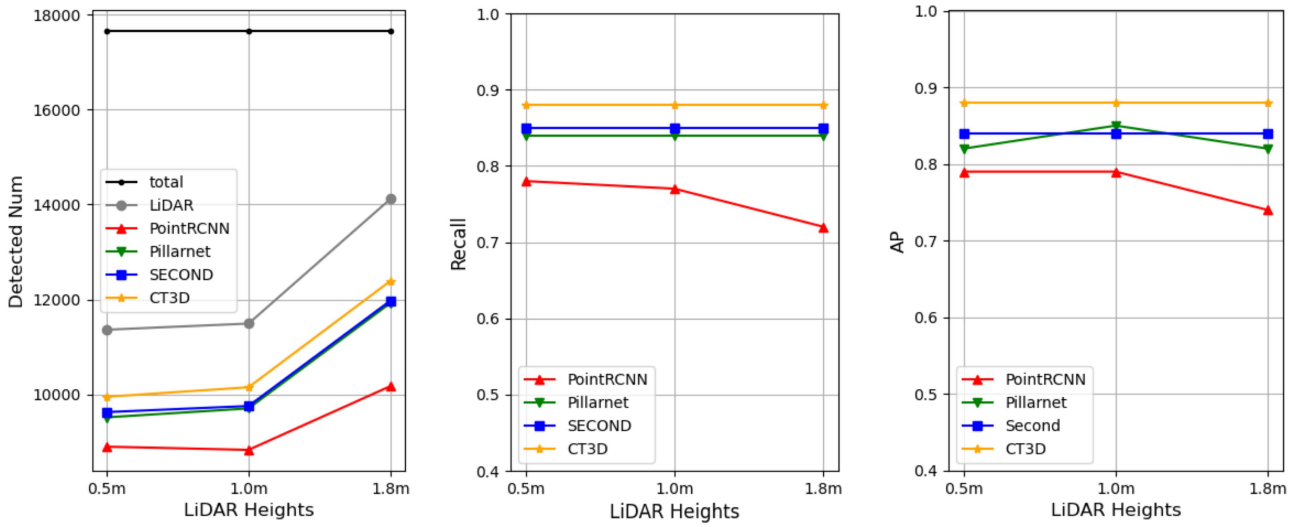

(a) The number of detected vehicles (b) The recall of algorithms (c) The AP of algorithms

Fig. 8. Performances of different 3D object detection algorithms under different LiDAR heights. (Numerical results are shown in the Appendix.).

considering more fine-grained information about the z-axis may be more vulnerable to the change in height. To gain valuable insights into the robustness of the 3D object detection algorithms across different data representation paradigms and backbone architectures, we chose 4 data representation paradigms and selected one algorithm for each paradigm. Specifically, we chose PointRCNN [21] for point-based data representation, Pillarnet [20] for pillar-based algorithms, SECOND [18] for voxel-based models, and CT3D [23] for innovative transformer-based two-stage detectors.

We still employed the aforementioned metrics with different ranges and importance levels on the evaluated data to obtain more fine-grained inference results of the algorithm models. The experiment divided the whole dataset into 4723 training frames and 2290 testing frames. The remaining 987 frames are not included in the algorithm testing stage for they have no vehicles in a certain range. We provide the 3D object detection results, including the recall rate and average precision, for the four 3D object detection models. It should be noted that the models were trained and tested by their corresponding training set and testing set with the same height. For example, the results of the "SECOND" model on the "1.0 m" dataset were estimated and evaluated on the "1.0 m" testing frames by the model of "SECOND" trained on the "1.0 m" training frames. All detailed results are shown in Tables VII, VIII and IX.

A. *Performance of Multiple Algorithms on Height3*

In Fig. 8(a), the numbers of detected vehicles by LiDAR sensors in the 2290 testing frames are consistent with the results in Section IV-B, where the height 1.8 m outperforms the other two heights.

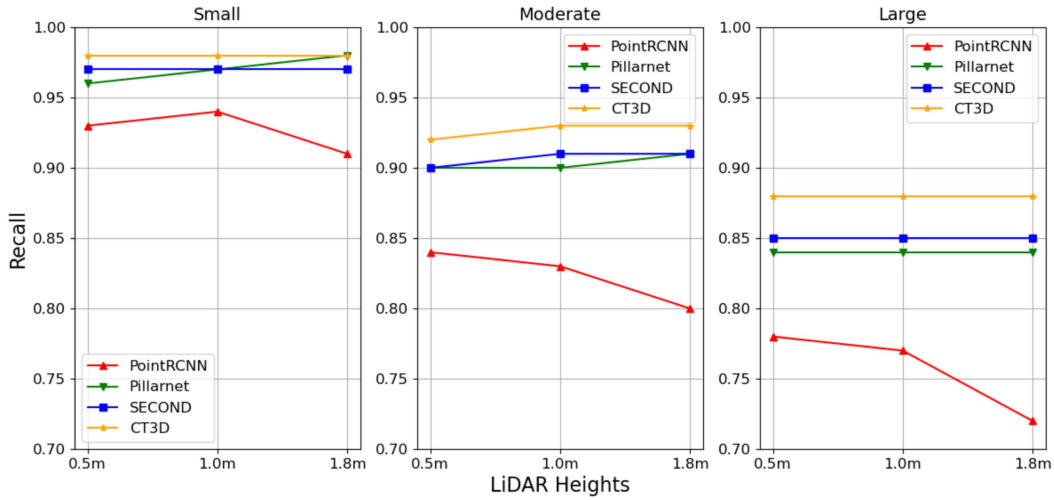

Fig. 9. Recall of four algorithms on different LiDAR heights and ranges (Numerical results are shown in the Appendix.)

We define a vehicle that was successfully detected by the algorithm model as the true positive (TP) vehicle estimated by the model. Specifically, we consider predicted true positive samples as those prediction boxes that exhibit an Intersection over Union (IoU) value of 0.7 or higher when compared to the ground truth boxes, and we exclude boxes with scores below 0.1 from the evaluation. It is worth noting that the detected vehicles of 3D object detection algorithms are always a subset of the detected vehicles by LiDAR sensors.

When considering the detected vehicles by different 3D object detection algorithms in Fig. 8(a), the transformer-based CT3D outperforms the other three algorithms. Pillarnet and SECOND have a similar number of detected vehicles, while the PointRCCN has the worst performance.

However, because the 1.8 m LiDAR captured the highest amount of vehicles, even if the PointRCNN has the worst performance, the number of detected vehicles of this algorithm in 1.8 m is still close to that of the best algorithm CT3D in 1.0 m. Therefore, we can conclude that even if the performances of different algorithms vary a lot, the main factor that influences their performance is the total number of detected vehicles by the LiDAR sensor, which is highly determined by its mounting height.

The recall rate of the algorithm's evaluation result is defined as:

$$Recall = \frac{TP}{LiDAR\ Detected\ Num}, \tag{2}$$

where "TP" aligns with its definition as mentioned before, and the "LiDAR detected num" is the number of detected vehicles by the LiDAR sensor.

The average precision (AP) is defined as:

$$AP = \frac{1}{40} \sum_{r \in R} \frac{TP}{TP + FP}, \tag{3}$$

where we use the "AP@R40" to calculate the "AP", and "R" represents a recall set containing 40 sequential recall points, and the "FP" means the number of false positive estimated vehicles.

Fig. 8(b) and (c) show the recall and AP variations of different algorithms with LiDAR heights respectively. The Pillarnet, SECOND, and CT3D are generally stable compared to PointRCNN. PointRCNN has a drop of performance in 1.8 m both in recall rate and AP. The decrease in the algorithm's performance due to the increase in height is abnormal. One possible reason is that when the LiDAR height increases to 1.8 m, the detected objects by the LiDAR sensor highly increase, and the number of points in each object decreases. For point-based methods, which directly process the data on the raw point cloud, the computational accuracy decreases.

As the performances of the other three algorithms are stable, we can conclude that except for the point-based algorithms, the other 3D object detection models are stable under the variation of point cloud shapes due to the changes in LiDAR heights.

TABLE III
RESOURCE COSTS OF DIFFERENT ALGORITHMS

Algorithm	Inference Time (ms)	Model Size (Mb)
PointRCNN	32.1	47
Pillarnet	6.8	126
Second	5.7	61
CT3D	24.0	84

Table III shows the inference time and the model size of each of the models on the Height3 dataset. The inference time is tested by one NVIDIA GeForce RTX 3090. Combined with the recall and AP, the Second model had a good trade-off between the cost of resources and the model performance.

B. Performance of Algorithms With Variations of Heights and Ranges

Fig. 9 shows the variation in the performance of different algorithms under different ranges. As the range expands, the performances of all algorithms decrease. In the "Large" range, except for the PointRCNN, the other three algorithms have stable performances under different ranges. In the other two ranges, there are some small variations in their performances. The same as the result in Section V-A, the PointRCNN always has a performance drop due to the height increases.

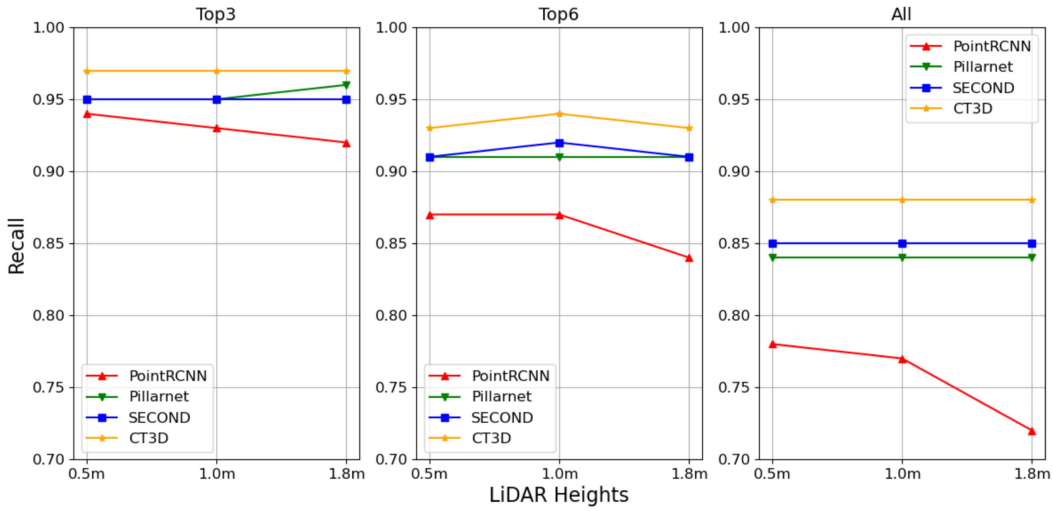

Fig. 10. Recall of four algorithms on different LiDAR heights and importance levels (Numerical results are shown in the Appendix.)

C. Performance of Algorithms With Variations of Heights and Importance Levels

Fig. 10 shows the variation in the performance of different algorithms under different importance levels. All models are excellent in estimating the "Top3" vehicles. The performances drop when it turns to "Top6" and "All" vehicles. This variation aligns with the trend of the detection ability of LiDAR sensors under different importance levels. The drop in performance of PointRCNN due to the increase of LiDAR height still remains apparent in different importance levels.

VI. Conclusion and Future Works

In general, this article examines the impact of different mounting heights of commercially available LiDARs on both the detection ability of LiDAR sensors and the performance of 3D vehicle detection algorithms. Based on the common mounting heights of LiDARs in production vehicles, we collected the Height3 dataset using LiDARs placed at heights of 0.5 m, 1.0 m, and 1.8 m. Through the analysis of the Height3 dataset, we found that the LiDAR mounted on the top of the vehicle exhibited the strongest perception capabilities, capturing the highest number of vehicles from the environment. However, there was little difference in the perception of the "Top3" and "Top6" vehicles among the LiDARs at different heights. The performances of the 3D vehicle detection algorithms were not significantly affected by the height at which the point cloud was captured, except for point-based methods. However, due to the larger number of vehicles detected by the 1.8 m LiDAR sensor, the algorithm was able to accurately detect more vehicles in the 1.8 m point cloud. Therefore, we can conclude that the evaluation results are mainly driven by the actual detected number of vehicles by the LiDAR sensor, which is highly determined by the occlusion of environmental objects.

Based on the above findings, we can make the following conclusions:

1) Choosing the vehicle's forehead as the preferred installation position for LiDAR is highly recommended. However, sometimes it is not able to mount the LiDAR sensor on the forehead due to some aesthetic requirements or industrial production requirements. Besides, lower-mounted LiDARs may be more sensible to the small objects close to the front of the vehicle, but further verification is needed. In these cases, there is not a big difference in the LiDAR perception capability to mount LiDAR sensors at other heights except for the forehead.
2) When considering the "Top3" vehicles in the environment, LiDAR sensors at all heights exhibit excellent perception capabilities. Therefore, installing a LiDAR at a lower position does not result in a significant decrease in perception capability when we only consider the vehicles posing threats to the ego vehicle.
3) Using point-based feature extraction methods is not recommended, as their performance is heavily influenced by the height of the LiDAR sensor. The other three algorithms demonstrate stable capabilities at different LiDAR heights. Therefore, it is free to choose based on the requirements for algorithm performance and resource cost.

Since all of our experiments are based on the simulated dataset, further validations in realistic datasets are suggested for vehicle designers.

Since real-world traffic scenarios are more complex than the ones studied in this experiment, future works can focus on investigating more intricate urban and rural environments, as well as incorporating a wider variety of object types, especially the VRUs (Vulnerable Road Users), such as pedestrians, bicycles, and so on. In addition, it is also of practical significance to explore the impact of more diverse LiDAR configurations on the perception capabilities of production vehicles. For example, studying different LiDAR rotation angles, the combined perception effects of multiple LiDAR sensors, and other related factors would be valuable areas of research.

Since LiDAR is not the only sensor in intelligent vehicles, we'd like to further research the impact of LiDAR's mounting height on multimodal perception. However, to simplify the big variations in other sensors' setups in different vehicle models, we envisioned using a unified monocular forward-facing camera, a fixed number and position of millimeter wave radars, and ultrasonic sensors to collect the data.

APPENDIX
TOTAL EXPERIMENT DATA

TABLE IV
LIDAR DETECTION RESULTS OF ALL VEHICLES

Ranges	Heights	0.5m	1.0m	1.8m
	Total	Number / LDR		
Small	17268	12638 / 0.73	12572 / 0.73	14739 / 0.85
Moderate	39455	26407 / 0.67	26216 / 0.66	32074 / 0.81
Large	54097	34296 / 0.63	34339 / 0.63	42185 / 0.78

TABLE V
LIDAR DETECTION RESULTS OF "TOP3" VEHICLES

Ranges	Heights	0.5m	1.0m	1.8m
	Total	Number / LDR		
Small	9949	9725 / 0.98	9730 / 0.98	9862 / 0.99
Moderate	13364	12900 / 0.97	12899 / 0.97	13135 / 0.98
Large	14522	13927 / 0.96	13925 / 0.96	14212 / 0.98

TABLE VI
LIDAR DETECTION RESULTS OF "TOP6" VEHICLES

Ranges	Heights	0.5m	1.0m	1.8m
	Total	Number / LDR		
Small	13661	11923 / 0.87	11732 / 0.86	12838 / 0.94
Moderate	20407	17444 / 0.85	17147 / 0.84	18824 / 0.92
Large	23303	19543 / 0.84	19267 / 0.83	21135 / 0.91

TABLE VII
DETECTION RESULTS OF 3D OBJECT DETECTION ALGORITHMS OF ALL VEHICLES

Ranges	Heights		0.5m					1.0m					1.8m				
	Total	Algorithms	LiDAR Detected					PointRCNN			Pillarnet		SECOND		CT3D		
Small	6692	Number	5042	4699	4864	4880	4926	5054	4743	4896	4900	4938	5821	5305	5690	5670	5706
		LDR/Recall	0.75	0.93	0.96	0.97	0.98	0.76	0.94	0.97	0.97	0.98	0.87	0.91	0.98	0.97	0.98
Moderate	13682	Number	9298	7849	8328	8397	8581	9371	7824	8468	8486	8722	11331	9031	10293	10299	10562
		LDR/Recall	0.68	0.84	0.90	0.90	0.92	0.68	0.83	0.90	0.91	0.93	0.83	0.80	0.91	0.91	0.93
Large	17641	Number	11364	8902	9519	9630	9952	11493	8835	9708	9758	10153	14120	10178	11929	11979	12394
		LDR/Recall	0.64	0.78	0.84	0.85	0.88	0.65	0.77	0.84	0.85	0.88	0.80	0.72	0.84	0.85	0.88

TABLE VIII
DETECTION RESULTS OF 3D OBJECT DETECTION ALGORITHMS OF "TOP3" VEHICLES

Ranges	Heights		0.5m					1.0m					1.8m				
	Total	Algorithms	LiDAR Detected					PointRCNN			Pillarnet		SECOND		CT3D		
Small	3704	Number	3628	3597	3599	3595	3614	3631	3589	3597	3593	3612	3670	3601	3640	3630	3647
		LDR/Recall	0.98	0.99	0.99	0.99	1.00	0.98	0.99	0.99	0.99	0.99	0.99	0.98	0.99	0.99	0.99
Moderate	4493	Number	4359	4221	4245	4234	4290	4365	4175	4240	4241	4301	4440	4180	4328	4287	4365
		LDR/Recall	0.97	0.97	0.97	0.97	0.98	0.97	0.96	0.97	0.97	0.99	0.99	0.94	0.97	0.97	0.98
Large	4763	Number	4600	4345	4380	4367	4442	4600	4288	4375	4389	4459	4694	4296	4490	4439	4534
		LDR/Recall	0.97	0.94	0.95	0.95	0.97	0.97	0.93	0.95	0.95	0.97	0.99	0.92	0.96	0.95	0.97

TABLE IX
DETECTION RESULTS OF 3D OBJECT DETECTION ALGORITHMS OF "TOP6" VEHICLES

Ranges	Heights		0.5m					1.0m					1.8m				
	Total	Algorithms	LiDAR Detected					PointRCNN		Pillarnet		SECOND	CT3D				
Small	5201	Number	4641	4448	4539	4551	4579	4573	4436	4501	4502	4525	4934	4706	4856	4846	4872
		LDR/Recall	0.89	0.96	0.98	0.98	0.99	0.88	0.97	0.98	0.98	0.99	0.95	0.95	0.98	0.98	0.99
Moderate	6882	Number	5946	5434	5602	5626	5710	5885	5351	5579	5600	5693	6447	5707	6104	6069	6200
		LDR/Recall	0.86	0.91	0.94	0.95	0.96	0.86	0.91	0.95	0.95	0.97	0.94	0.89	0.95	0.94	0.96
Large	7538	Number	6418	5607	5823	5846	5973	6358	5515	5807	5845	5972	6989	5875	6380	6347	6517
		LDR/Recall	0.85	0.87	0.91	0.91	0.93	0.84	0.87	0.91	0.92	0.94	0.93	0.84	0.91	0.91	0.93

REFERENCES

[1] R. Roriz, J. Cabral, and T. Gomes, "Automotive LiDAR technology: A survey," *IEEE Trans. Intell. Transp. Syst.*, vol. 23, no. 7, pp. 6282–6297, Jul. 2022.

[2] M. Buehler, K. Iagnemma, and S. Singh, *The DARPA Urban Challenge: Autonomous Vehicles in City Traffic*, 1st ed. Berlin, Germany: Springer, 2009.

[3] C. Urmson et al., "High speed navigation of unrehearsed terrain: Red team technology for grand challenge2004," Robotics Institute, Carnegie Mellon University, Pittsburgh, PA, USA, Tech. Rep. CMU-RI-04-37, 2004.

[4] B. L. Stann, J. F. Dammann, and M. M. Giza, "Progress on MEMS-Scanned Ladar," *Proc. SPIE*, vol. 9832, pp. 197–205, 2016.

[5] C. Zhang, S. Lindner, I. M. Antolović, J. M. Pavia, M. Wolf, and E. Charbon, "A 30-frames/s, 252×144 SPAD flash LiDAR with 1728 dual-clock 48.8-ps TDCs, and pixel-wise integrated histogramming," *IEEE J. Solid-State Circuits*, vol. 54, no. 4, pp. 1137–1151, Apr. 2019.

[6] D. Wang, C. Watkins, and H. Xie, "MEMS mirrors for LiDAR: A review," *Micromachines*, vol. 11, no. 5, 2020, Art. no. 456.

[7] H. W. Yoo et al., "MEMS-based LiDAR for autonomous driving," *e i Elektrotechnik und Informationstechnik*, vol. 135, no. 6, pp. 408–415, 2018.

[8] J. Lemmetti, N. Sorri, I. Kallioniemi, P. Melanen, and P. Uusimaa, "Long-range all-solid-state flash LiDAR sensor for autonomous driving," *Proc. SPIE*, vol. 11668, pp. 99–105, 2021.

[9] R. Halterman and M. Bruch, "Velodyne HDL-64E LiDAR for Unmanned Surface Vehicle Obstacle Detection," *Proc. SPIE*, vol. 7692, pp. 123–130, 2010.

[10] C.-P. Hsu et al., "A review and perspective on optical phased array for automotive LiDAR," *IEEE J. Sel. Topics Quantum Electron.*, vol. 27, no. 1, pp. 1–16, Jan./Feb. 2021.

[11] Z. Liu, M. Arief, and D. Zhao, "Where should we place LiDARs on the autonomous vehicle? - An optimal design approach," in *Proc. IEEE Int. Conf. Robot. Automat.*, 2019, pp. 2793–2799.

[12] S. Mou, Y. Chang, W. Wang, and D. Zhao, "An optimal LiDAR configuration approach for self-driving cars," 2018, *arXiv:1805.07843*.

[13] F. Berens, S. Elser, and M. Reischl, "Genetic algorithm for the optimal LiDAR sensor configuration on a vehicle," *IEEE Sensors J.*, vol. 22, no. 3, pp. 2735–2743, Feb. 2022.

[14] T.-H. Kim and T.-H. Park, "Placement optimization of multiple lidar sensors for autonomous vehicles," *IEEE Trans. Intell. Transp. Syst.*, vol. 21, no. 5, pp. 2139–2145, May 2020.

[15] S. Manivasagam et al., "LiDARsim: Realistic LiDAR simulation by leveraging the real world," in *Proc. IEEE/CVF Conf. Comput. Vis. Pattern Recognit.*, 2020, pp. 11164–11173.

[16] P. Jabłoński, J. Iwaniec, and W. Zabierowski, "Comparison of pedestrian detectors for LiDAR sensor trained on custom synthetic, real and mixed datasets," *Sensors*, vol. 22, no. 18, 2022, Art. no. 7014.

[17] Y. Zhou and O. Tuzel, "VoxelNet: End-to-end learning for point cloud based 3D object detection," in *Proc. IEEE/CVF Conf. Comput. Vis. Pattern Recognit.*, 2018, pp. 4490–4499.

[18] Y. Yan, Y. Mao, and B. Li, "Second: Sparsely embedded convolutional detection," *Sensors*, vol. 18, no. 10, 2018, Art. no. 3337.

[19] A. H. Lang, S. Vora, H. Caesar, L. Zhou, J. Yang, and O. Beijbom, "Pointpillars: Fast encoders for object detection from point clouds," in *Proc. IEEE/CVF Conf. Comput. Vis. Pattern Recognit.*, 2019, pp. 12689–12797.

[20] G. Shi, R. Li, and C. Ma, "PillarNet: Real-time and high-performance pillar-based 3D object detection," in *Proc. Eur. Conf. Comput. Vis.*, 2022, pp. 35–52.

[21] S. Shi, X. Wang, and H. Li, "PointRCNN: 3D object proposal generation and detection from point cloud," in *Proc. IEEE/CVF Conf. Comput. Vis. Pattern Recognit.*, 2019, pp. 770–779.

[22] T. Yin, X. Zhou, and P. Krahenbuhl, "Center-based 3D object detection and tracking," in *Proc. IEEE/CVF Conf. Comput. Vis. Pattern Recognit.*, 2021, pp. 11784–11793.

[23] H. Sheng et al., "Improving 3D object detection with channel-wise transformer," in *Proc. IEEE/CVF Int. Conf. Comput. Vis.*, 2021, pp. 2723–2732.

[24] C. R. Qi, O. Litany, K. He, and L. J. Guibas, "Deep hough voting for 3D object detection in point clouds," in *Proc. IEEE/CVF Int. Conf. Comput. Vis.*, 2019, pp. 9276–9285.

[25] I. Misra, R. Girdhar, and A. Joulin, "An end-to-end transformer model for 3D object detection," in *Proc. IEEE/CVF Int. Conf. Comput. Vis.*, 2021, pp. 2886–2897.

[26] C. R. Qi, X. Chen, O. Litany, and L. J. Guibas, "Imvotenet: Boosting 3D object detection in point clouds with image votes," in *Proc. IEEE/CVF Conf. Comput. Vis. Pattern Recognit.*, 2020, pp. 4403–4412.

[27] Y. Zheng, Y. Duan, J. Lu, J. Zhou, and Q. Tian, "HyperDet3D: Learning a scene-conditioned 3D object detector," in *Proc. IEEE/CVF Conf. Comput. Vis. Pattern Recognit.*, 2022, pp. 5575–5584.

[28] J. Deng, S. Shi, P. Li, W. Zhou, Y. Zhang, and H. Li, "Voxel R-CNN: Towards high performance voxel-based 3D object detection," in *Proc. AAAI Conf. Artif. Intell.*, 2021, pp. 1201–1209.

[29] H. Kuang, B. Wang, J. An, M. Zhang, and Z. Zhang, "Voxel-FPN: Multi-scale voxel feature aggregation for 3D object detection from LiDAR point clouds," *Sensors*, vol. 20, no. 3, 2020, Art. no. 704.

[30] S. Shi et al., "PV-RCNN: Point-voxel feature set abstraction for 3D object detection," in *Proc. IEEE/CVF Conf. Comput. Vis. Pattern Recognit.*, 2020, pp. 10526–10535.

[31] S. Shi et al., "PV-RCNN : Point-voxel feature set abstraction with local vector representation for 3D object detection," *Int. J. Comput. Vis.*, vol. 131, no. 2, pp. 531–551, 2023.

[32] E. Romera, J. M. Alvarez, L. M. Bergasa, and R. Arroyo, "ERFNet: Efficient residual factorized convnet for real-time semantic segmentation," *IEEE Trans. Intell. Transp. Syst.*, vol. 19, no. 1, pp. 263–272, Jan. 2018.

[33] H. Zhao, J. Shi, X. Qi, X. Wang, and J. Jia, "Pyramid scene parsing network," in *Proc. IEEE Conf. Comput. Vis. Pattern Recognit.*, 2017, pp. 2881–2890.

[34] Y. Qian, L. Deng, T. Li, C. Wang, and M. Yang, "Gated-residual block for semantic segmentation using RGB-D data," *IEEE Trans. Intell. Transp. Syst.*, vol. 23, no. 8, pp. 11836–11844, Aug. 2022.

[35] G. Zamanakos, L. Tsochatzidis, A. Amanatiadis, and I. Pratikakis, "A comprehensive survey of LiDAR-based 3D object detection methods with deep learning for autonomous driving," *Comput. Graph.*, vol. 99, pp. 153–181, 2021.

[36] C. R. Qi, H. Su, K. Mo, and L. J. Guibas, "PointNet: Deep learning on point sets for 3D classification and segmentation," in *Proc. IEEE Conf. Comput. Vis. Pattern Recognit.*, 2017, pp. 652–660.

[37] D. Lu, Q. Xie, M. Wei, L. Xu, and J. Li, "Transformers in 3D point clouds: A survey," 2022, *arXiv:2205.07417*.

[38] A. Geiger, P. Lenz, C. Stiller, and R. Urtasun, "Vision meets robotics: The kitti dataset," *Int. J. Robot. Res.*, vol. 32, no. 11, pp. 1231–1237, 2013.

[39] H. Caesar et al., "nuScenes: A multimodal dataset for autonomous driving," in *Proc. IEEE/CVF Conf. Comput. Vis. Pattern Recognit.*, 2020, pp. 11618–11628.

[40] P. Sun et al., "Scalability in perception for autonomous driving: Waymo open dataset," in *Proc. IEEE/CVF Conf. Comput. Vis. Pattern Recognit.*, 2020, pp. 2443–2451.

[41] J. Mao et al., "One million scenes for autonomous driving: Once dataset," 2021, *arXiv:2106.11037*.
[42] A. Patil, S. Malla, H. Gang, and Y.-T. Chen, "The H3D dataset for full-surround 3D multi-object detection and tracking in crowded urban scenes," in *Proc. IEEE Int. Conf. Robot. Automat.*, 2019, pp. 9552–9557.
[43] M.-F. Chang et al., "Argoverse: 3D tracking and forecasting with rich maps," in *Proc. IEEE/CVF Conf. Comput. Vis. Pattern Recognit.*, 2019, pp. 8740–8749.
[44] F. Berens, S. Elser, and M. Reischl, "Generation of synthetic point clouds for MEMS LiDAR sensor," 2022, *arXiv:19615563.v2*.

Kezhi Li is currently working toward the undergraduation degree with the University of Michigan-Shanghai Jiao Tong University Joint Institute, Shanghai Jiao Tong University, Shanghai, China. His main interests include electric and computer engineering. His research interests include autonomous driving, machine learning, and robotic technology.

Yeqiang Qian (Member, IEEE) received the Ph.D. degree in control science and engineering from Shanghai Jiao Tong University, Shanghai, China, in 2020. He is currently a Postdoctoral Fellow with the Global Institute of Future Technology, Shanghai Jiao Tong University. His main research interests include computer vision, pattern recognition, machine learning, and their applications in intelligent transportation systems.

Chunxiang Wang received the Ph.D. degree in mechanical engineering from the Harbin Institute of Technology, Harbin, China, in 1999. She is currently an Associate Professor with the Department of Automation, Shanghai Jiao Tong University, Shanghai, China. Her research interests include robotic technology and electromechanical integration.

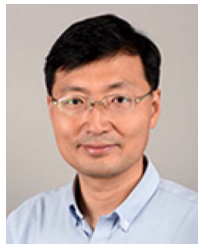

Ming Yang (Member, IEEE) received the master's and Ph.D. degrees from Tsinghua University, Beijing, China, in 1999 and 2003, respectively. He is currently a Full-Tenure Professor with Shanghai Jiao Tong University, Shanghai, China, and the Deputy Director of the Innovation Center of Intelligent Connected Vehicles. He has been working in the field of intelligent vehicles for more than 20 years. He participated in several related research projects, such as the THMR-V project (the first intelligent vehicle in China), European CyberCars and CyberMove projects, CyberC3 project, CyberCars-2 project, and ITER Transfer Cask Project, AGV.